EUROPHYSICS LETTERS 15 July 2000

Europhys. Lett., **51** (2), pp. 154–160 (200)

Surface effects on spinodal decomposition of incompressible binary fluid mixtures

H. Tanaka and T. Araki

Institute of Industrial Science, University of Tokyo - Meguro-ku, Tokyo 153-8505, Japan

(received 8 February 2000; accepted in final form 16 May 2000)

PACS. 64.75.+g – Solubility, segregation, and mixing; phase separation.
PACS. 68.45.Gd – Wetting.
PACS. 47.20.Dr – Surface-tension-driven instability.

Abstract. – We demonstrate the first three-dimensional simulations of bicontinuous spinodal decomposition of incompressible binary fluid mixtures in a confined geometry. We find that after an initial transient the thickness of a wetting layer L grows with time t as $L \sim t^{1/3}$ by a diffusion process and later as $L \sim t$ by a hydrodynamic one. We confirm that the hydrodynamic pumping of fluid via bicontinuous tubes plays dominant roles in the late-stage thickening dynamics of a wetting layer. A domain connected to the wetting layer grows faster than in bulk, which is suggestive of the hydrodynamic origin of the fast-mode kinetics found by Wiltzius and Cumming.

During phase separation of a binary mixture [1–3], the composition difference between the two phases increases with time until the system reaches its local equilibrium. When a mixture is in contact with a solid wall, the difference in interactions with the wall between the two components leads to wetting phenomena [4, 5]. Recently, the interplay between phase separation and wetting phenomena has attracted considerable attention from both the scientific and the industrial viewpoints [6–8]. This interest partly comes from the fact that in real experiments phase separation can never be free from surface effects. Further, there remain a few unsolved fundamental problems: i) How does the symmetry-breaking field make phase separation anisotropic? ii) How long-range are surface effects on the phase-separation morphology? iii) How do the surface effects affect the dynamics of domain coarsening? Here it should be noted that the answers to all these questions are crucially dependent upon whether a system is a solid mixture or a fluid mixture.

It was established experimentally that the symmetry-breaking surface field causes a strongly anisotropic surface composition wave near the surfaces [9, 10]. This behavior was also studied by numerical simulations in the framework of a solid model (model B) [11–14], where diffusion is the only process of material transport. Although the basic features of wetting effects on phase separation in a solid model have been clarified on a satisfactory level, the roles of hydrodynamic effects [1, 3, 15] are still far from being completely understood: For example, the fast-mode kinetics found by Wiltzius and Cumming [16] still remains as an unsolved problem [8, 17], although there are some attempts to explain this unusual behavior [14, 18–21]. Thus, the study of hydrodynamic effects on phase separation under wetting is necessary for a better understanding of complex pattern evolution of fluid phase separation in a confined geometry [14, 19, 22–26]. Marko [14] and one of the authors (HT) [19] suggested, using the scaling analysis, that the growth of the wetting layer in a fluid mixture is characterized by

the same exponent as the bulk domains. For 2D, Chen and Chakrabarti confirmed this by the first intensive numerical study of hydrodynamic effects on wetting.

In this letter, we study fluid phase separation under the influence of surface fields by using three-dimensional (3D) numerical simulations, to gain a new insight into the problem. Although there are some studies on two-dimensional (2D) fluid phase separation under wetting effects [27,28], it is expected from the case of bulk phase separation that the behavior in 3D [15] is even qualitatively different from that in 2D [29].

The basic Langevin equations describing the dynamics of a fluid model (model H in the Hohenberg-Halperin notation) are [1, 2]

$$\frac{\partial}{\partial t}\phi = -\vec{\nabla}\cdot(\phi\vec{v}) + L_\xi \nabla^2 \frac{\delta}{\delta\phi}(\beta H) + \theta, \tag{1}$$

$$\rho\frac{\partial}{\partial t}\vec{v} = \vec{F}_\phi - \vec{\nabla}p + \eta\nabla^2\vec{v} + \vec{\zeta}, \tag{2}$$

where ϕ is the composition, $\vec{v}$ is the velocity, $\beta = 1/k_{\rm B}T$ ($k_{\rm B}$: Boltzmann's constant), ρ is the density, η is the viscosity, and θ and $\vec{\zeta}$ are thermal noises. The pressure p is determined to satisfy the incompressibility condition $\vec{\nabla}\cdot\vec{v} = 0$. Here H is the Ginzburg-Landau–type Hamiltonian, which includes the surface contribution due to the existence of a wall at $z = 0$, $f_{\rm s}(\phi) = a\phi - (b/2)\phi^2$ (a and b are constants depending upon the surface properties) [13]:

$$\beta H = \int_{z\geq 0} {\rm d}\vec{r}\ \left[-\frac{1}{2}\tau\phi^2 + \frac{1}{4}u\phi^4 + \frac{1}{2}K|\vec{\nabla}\phi|^2 + f_{\rm s}(\phi)\delta(z)\right]. \tag{3}$$

In eq. (2), $\vec{F}_\phi$ is the thermodynamic force density acting on the fluid due to the fluctuations of the composition ϕ and $\vec{F}_\phi = -\phi\vec{\nabla}\mu = -\vec{\nabla}\pi + k_{\rm B}TK\phi\vec{\nabla}\nabla^2\phi$ (π: osmotic pressure), where $\mu = \delta H/\delta\phi$ is the chemical potential.

In the simulation, we scale length and time, respectively, by the correlation length of composition fluctuations ξ [$= (K/\tau)^{1/2}$] and its lifetime $\tau_\xi = \xi^2/D_\xi$, where D_ξ is the renormalized diffusion constant given by $D_\xi = \tau L_\xi$. After scaling length and time and neglecting noises, eq. (2) becomes $\partial\vec{V}/\partial t = \Gamma\vec{F} - \vec{\nabla}P + \Xi\nabla^2\vec{V}$, where $\vec{F}$ and $\vec{V}$ are the scaled $\vec{F}_\phi$ and $\vec{v}$, respectively. Here $\Gamma = \frac{\tau\phi_{\rm e}^2\tau_\xi^2}{\rho\beta\xi^2}$, where $\pm\phi_{\rm e}$ are final equilibrium compositions, $P = \frac{\tau_\xi^2}{\rho\xi^2}p$, and $\Xi = \frac{\eta\tau_\xi}{\rho\xi^2}$. Then, the fluidity parameter R is defined as

$$R = \frac{\Gamma}{\Xi} = \frac{\tau\phi_{\rm e}^2\tau_\xi}{\eta\beta} = 6\pi\tau\phi_{\rm e}^2\xi^3 = 18\pi\sigma\xi^2\beta, \tag{4}$$

where σ is the interface tension and the relation $\sigma/k_{\rm B}T = \frac{1}{3}\tau\xi\phi_{\rm e}^2$ is used. This R is a measure of the relative importance of the streaming term *vs.* the diffusion term. For 3D, R is a universal constant near a critical point [3] and estimeted as $R = 18\pi A_\sigma = 5$–10 since $\sigma = A_\sigma k_{\rm B}T/\xi^2$, where A_σ is a universal constant and $A_\sigma = 0.1$–0.2.

We consider a symmetric [50:50] mixture of A and B. The solid surface that favours A more than B is introduced at $z = 0$ by $f_{\rm s}(\phi)$ with $a = b = -1$, which corresponds to a "complete wetting" condition [4]. Here the positive ϕ means A-rich. The scaled equations are solved by the Euler method under an incompressibility condition $\vec{\nabla}\cdot\vec{V} = 0$ with the boundary conditions of $V_z = 0$ and $\partial\mu/\partial z = 0$ at $z = 0$ and with periodic boundary conditions along x and y directions. The system size was $64\times64\times64$ for 3D. We choose the grid size $\Delta x = \Delta y = \Delta z = 1$ and the time step $\Delta t = 0.01$ to ensure the numerical stability. We do not use the steady-state approximation ($\partial\vec{V}/\partial t = 0$) to handle the non-periodic boundary condition

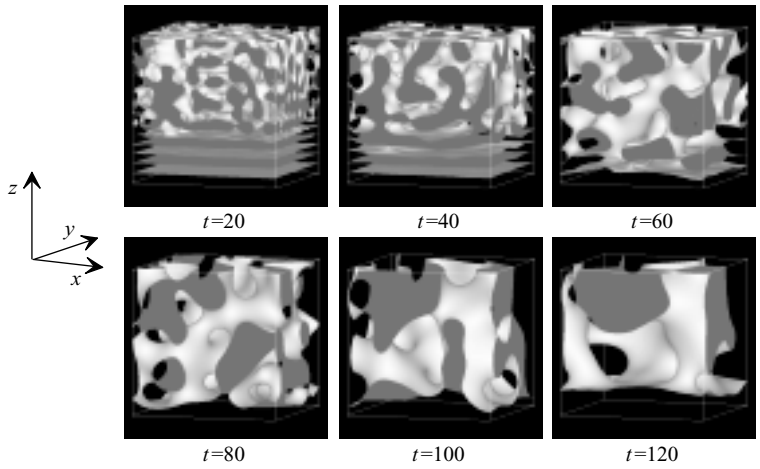

Fig. 1 – 3D pattern evolution during spinodal decomposition under the influence of wetting to the solid wall at the bottom ($z = 0$). Here $\Gamma = 10$ and $\Xi = 1$.

imposed by the wall. Instead, the velocity fields are calculated in real space by solving $\partial\vec{V}/\partial t = \Gamma\vec{F} - \vec{\nabla}P + \Xi\nabla^2\vec{V}$. We calculate $\Gamma\vec{F} - \vec{\nabla}P$ by an inverse Fourier transformation of $\boldsymbol{D}_q \cdot \Gamma\vec{F}_q$, where $\boldsymbol{D}_q = \boldsymbol{I} - \vec{q}\vec{q}/q^2$ (note that $\vec{\nabla}\cdot(\Gamma\vec{F} - \vec{\nabla}P) = 0$ since $\vec{\nabla}\cdot\vec{V} = 0$). Random noises of ϕ (10^{-3} in amplitude) are introduced only at $t = 0$, while velocity noises are not.

Figure 1 shows the overall pattern evolution during spinodal decomposition under the surface fields of a wall set at the bottom ($z = 0$). In this figure, we display an interface of $\phi = 0$. It should be noted that before $t \leq 40$ a sharp interface is not formed yet, although the figure gives us an impression of the existence of a sharp interface. Initially, the composition wave, or the composition oscillation along the z direction, is observed near the wall, as well known [6–14]. Then, we can see sequentially the destruction of the composition wave, the formation of a wetting layer of the A-rich phase, and its thickening. The temporal change in $\bar{\phi}(z) = (1/64^2)\int\phi(x,y,z)\mathrm{d}x\mathrm{d}y$ are shown for a solid and a fluid mixture, respectively, in figs. 2(a) and (b). Note that the lifetime of the composition wave is much shorter in a fluid mixture than in a solid mixture.

Figures 3(a) and (b) show the temporal change in the wetting layer thickness $L(t)$ for both solid and fluid mixtures, respectively, for $\Xi = 1$ and $\Xi = 5$. For solid mixtures the wetting layer grows as $L \sim t^{1/3}$ after an initial transient rapid growth of a wetting layer, which depends on surface parameters (a, b), while for fluid mixtures it initially follows the behavior of solid mixtures, but later grows as $L = k(t - t_\mathrm{c})$. Here t_c is the onset time of hydrodynamic effects, at which $|\vec{v}|$ in bulk reaches its stationary value of $|\vec{v}| \sim \sigma/\eta$ [15]. Consistently with this, k was found to be proportional to Γ/Ξ ($\propto \sigma/\eta$). This late-stage linear growth is quite consistent with the experimental observation [19, 30] and the theoretical prediction [$L \sim (\sigma/\eta)t$] [14, 19, 21]. The differences in k and t_c between a case of $\Xi = 1$ and that of $\Xi = 5$ may be due to the difference in the strength of the inertia effects. This point remains as a future problem. The deviation from the t-linear law for $L > 15$ may be due to the finite-size effects.

To see these hydrodynamic effects on the coarsening behavior in a more evident way, we display the flow fields along the z direction in fig. 4. In the vertical view (a), we can clearly see the directional flow toward the wetting layer via tubes connected to it. This clearly indicates that the hydrodynamic transport of the more wettable phase from the bulk to the wetting

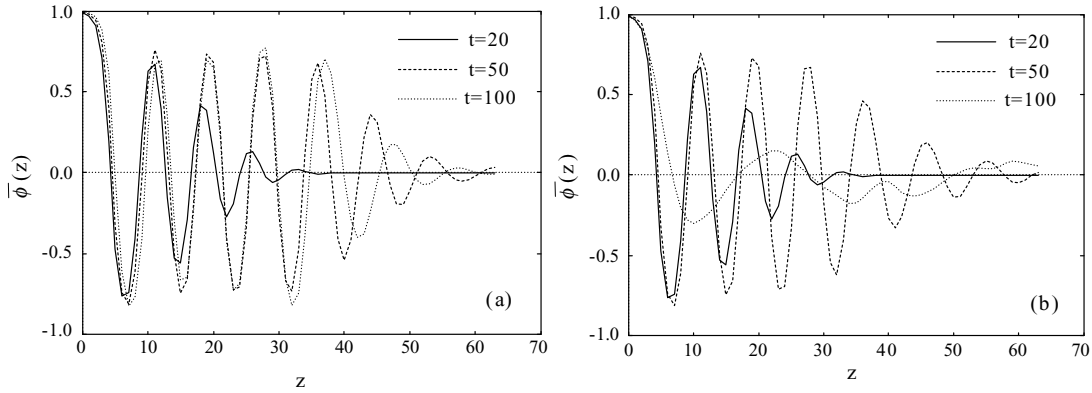

Fig. 2 – Temporal change in concentration profile along z (averaged over x and y directions), $\bar{\phi}(z)$, for (a) a solid model and (b) a fluid model ($\Gamma = 10$ and $\Xi = 1$).

layer is a dominant process in the late-stage thickening of a wetting layer. In the horizontal view (b), we can also see the hydrodynamic pumping of the more wettable phase into the wetting layer. It should be noted that this flow spreads on the wetting layer, which causes the radial thickening of a part of a fluid tube connected to the wetting layer. This leads to the faster coarsening near the wetting layer, as described later (see figs. 6(a) and (b)). All these effects are due to that a pressure in fluid tubes of a bulk bicontinuous structure is higher than that in a wetting layer by $\sim \sigma/a_{\rm tube}$ ($a_{\rm tube}$: radius of fluid tubes) [19, 21].

Here we discuss i) the formation of a composition wave, ii) its disappearance, and iii) the thickening dynamics of a wetting layer. As can be seen clearly in figs. 1 and 2, a composition wave is first formed near the surface. This process is dominated by the diffusion process. The physical origin of the appearance of the composition wave near the surface has already been discussed intensively [6–14]. This anisotropic composition wave is one of the most drastic effects of the symmetry-breaking surface field on the early-stage spinodal decomposition.

Later on, it is gradually destroyed by the growing bulk composition fluctuations that are basically isotropic. Since hydrodynamic effects produce the material flow toward the wall, this destruction dynamics of the composition wave is significantly accelerated for a fluid

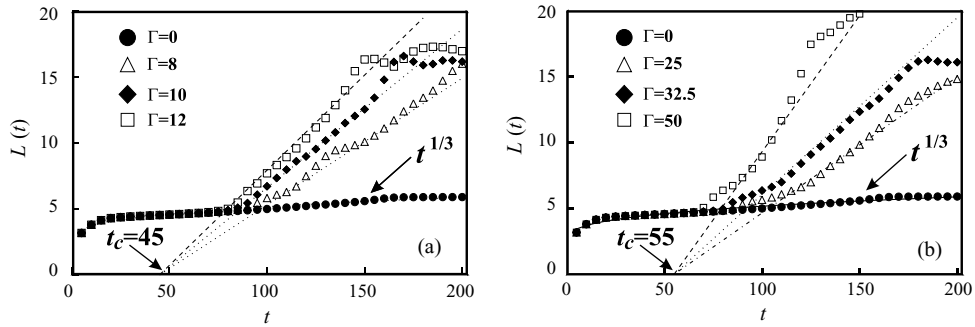

Fig. 3 – Temporal change in the thickness L of wetting layer for a solid ($\Gamma = 0$) and fluid model ($\Gamma \neq 0$). (a) $\Xi = 1$. The curves are $L = 2.43 + 0.587t^{1/3}$ and $L = 0.0120(\Gamma/\Xi)(t - t_{\rm c})$; (b) $\Xi = 5$. The curves are $L = 2.43 + 0.587t^{1/3}$ and $L = 0.0206(\Gamma/\Xi)(t - t_{\rm c})$.

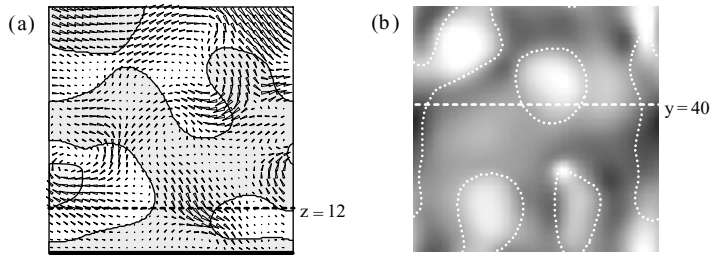

Fig. 4 – (a) Flow fields at $t = 80$ in a plane ($y = 40$) perpendicular to the wall at bottom (drawn by the thick line). The gray phase is an A-rich phase. (b) Flow fields at $t = 80$ near the wall in a plane ($z = 12$) parallel to the wall. The white dotted curves indicate the domain interface. The contrast of the gray-scale image represents V_z: white contrast means flow toward the wall, while black contrast means flow in the opposite direction. Here $\Gamma = 10$ and $\Xi = 1$.

system compared to a solid system (see fig. 2). As the interface becomes sharper with time, the average velocity of the hydrodynamic flow increases, following the relation $|\vec{v}| = v \sim (\Delta\phi)^2$ [31], where $\Delta\phi$ is the composition difference between the two phases. The hydrodynamic flow from bulk to the higher-order layers destabilizes the layer structures. Accordingly, the higher-order layers are sequentially destroyed one by one from $t \sim 30$, and eventually a single wetting layer is formed around $t \sim 70$ (see figs. 1 and 2). Then the hydrodynamic transport of the more wettable phase via fluid tubes becomes a dominant process of the thickening of the wetting layer and the thickness starts to increase linearly with time by a "hydrodynamic pumping" mechanism [19, 21]. It should be noted that bicontinuous fluid tubes are always connected directly and perpendicularly to the surface wetting layer in the late stage (see fig. 1). This destruction of a composition wave and the resulting formation of a single wetting layer are required for the switching of the thickening mechanism of a wetting layer from a diffusional to a hydrodynamic one.

Next we point out that the hydrodynamic thickening of the wetting layer is too quick for a diffusion process to follow and this retardation of diffusion brings the system out of equilibrium [20]. To see this effect, we plot in fig. 5 the diffusion flux $|\vec{\nabla}\mu|$ in bulk and that in the wetting layer, together with the hydrodynamic flux $|\phi\vec{v}|$. For a solid mixture, $|\vec{\nabla}\mu|$

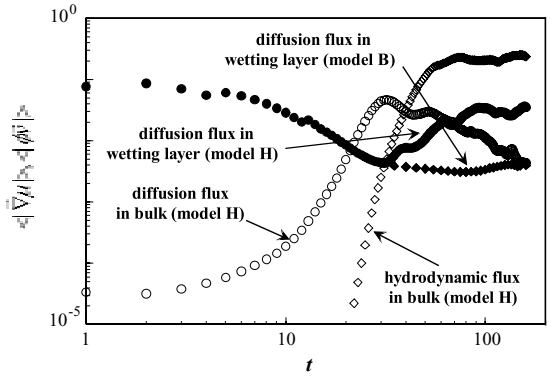

Fig. 5 – Temporal change in diffusion flux in the wetting layer and in bulk together with the growth of the hydrodynamic flux in bulk. Here $\Gamma = 10$ and $\Xi = 1$.

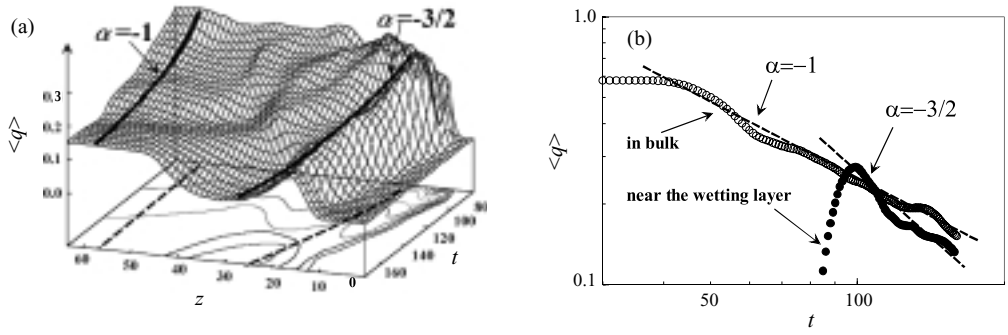

Fig. 6 – (a) Time development of $\langle q(z)\rangle$. The coarsening near the wall is considerably faster than that in bulk. Here $\Gamma = 10$ and $\Xi = 1$. (b) Temporal change in $\langle q\rangle$ near the wetting layer and in bulk.

in the wetting layer monotonically decreases with time, while for a fluid mixture it initially decreases with time, but starts to increase around $t \sim 30$. At this time, the hydrodynamic flow from bulk to the higher-order layers is initiated, as described before, and it also affects the primary wetting layer because of its long-range nature. Since diffusion cannot follow this quick hydrodynamic process, the wetting layer starts to become out of equilibrium, which enhances the diffusion flux in the wetting layer for $t > 70$. The absence of such effects in a solid system (model B [2]), which is confirmed by our simulation (see fig. 5), clearly indicates that this is not due to the surface-potential effects, but to the hydrodynamic effects. This retardation of the diffusion makes the phase-separated phases metastable or unstable again and may even lead to a drastic phenomenon of "double phase separation" [20, 31, 32].

Finally we discuss the faster coarsening near the wetting layer than in the bulk, in relation to the above-described effects. We plot the temporal change in the characteristic wave number $\langle q(z)\rangle$ in fig. 6(a). Here $\langle q(z)\rangle = \int \mathrm{d}q_x \mathrm{d}q_y q_2 S(q_x, q_y, z) / \int \mathrm{d}q_x \mathrm{d}q_y S(q_x, q_y, z)$, where S is the structure factor in a xy-plane and $q_2^2 = q_x^2 + q_y^2$. We can clearly see that the domain coarsening near the wetting layer is faster than that in bulk. Figure 6(b) shows the temporal change in $\langle q\rangle$ of bulk (averaged around $z \sim 57$) and the local minimum $\langle q\rangle$ near the surface of the wetting layer (see the thick solid and dashed curves in fig. 6(a)). The coarsening in bulk is well described by $\langle q\rangle \sim t^{-1}$ for $t \geq t_c (= 45)$, which is typical of 3D spinodal decomposition of fluid mixtures. Note that a hydrodynamic transport exceeds a diffusional one for $t \geq t_c$ (see fig. 5). On the other hand, the fast domain coarsening near the wall can be approximated by $\langle q\rangle \sim t^{-3/2}$. This faster coarsening near the surface is suggestive of the physical origin of the fast-mode kinetics ($\langle q\rangle \sim t^{-3/2}$) observed by Wiltzius and Cumming [16]; namely, the hydrodynamic-pumping mechanism should be responsible for the fast-mode kinetics [19, 21]. A similar behavior was also observed for different (Γ, Ξ) and (a, b), which indicates the general nature of this behavior. However, the power law regime is too short for a conclusive argument and the question of whether it is transient or truly asymptotic also remains as a future problem. Thus, further studies are required for the unambiguous determination of the physical origin of this fast-growth mode.

In summary, we demonstrate three-dimensional simulations of spinodal decomposition of critical fluid mixtures under the influence of symmetry-breaking surface fields. The wetting-layer thickness grows as $L \sim t^{1/3}$ initially and then as $L \sim t$ in the late stage. We confirm that the hydrodynamic pumping mechanism of fluid tubes plays a dominant role in this late-stage thickening dynamics of wetting layers. The late-stage growth exponent for the wetting layer is found to be the same as that for bulk. This is basically consistent with simulation results

of a 2D fluid mixture [28]. We also find that the wetting effects accelerate the hydrodynamic domain coarsening near the wall. This fast surface coarsening is suggestive of the physical mechanism of the fast-mode kinetics found by Wiltzius and Cumming [16]. Since diffusion cannot follow this fast coarsening, the domains also become weakly out of equilibrium.

REFERENCES

[1] Gunton J. D., San M. Miguel and Sahni P., in *Phase Separation and Critical Phenomena*, edited by Domb C. and Lebowitz J. H., Vol. **8** (Academic, London) 1983.
[2] Hohenberg P. C. and Halperin B. I., *Rev. Mod. Phys.*, **49** (1976) 435.
[3] Bray A. J., *Adv. Phys.*, **43** (1994) 357.
[4] Cahn J. W., *J. Chem. Phys.*, **66** (1977) 3667.
[5] See, *e.g.*, de Gennes P. G., *Rev. Mod. Phys.*, **57** (1985) 827.
[6] See, *e.g.*, Krausch G., *Mater. Sci. Eng. Res.*, **14** (1995) 1.
[7] Puri S. and Frisch H. L., *J. Phys. Condens. Matter*, **9** (1997) 2109.
[8] Binder K., *J. Non-Equilib. Thermodyn.*, **23** (1998) 1.
[9] Jones R. A. L., Norton L. J., Kramer E. J., Bates F. S. and Wiltzius P., *Phys. Rev. Lett.*, **66** (1991) 1326.
[10] Krausch G., Dai C., Kramer E. J. and Bates F. S., *Phys. Rev. Lett.*, **71** (1993) 3669; Krausch G., Dai C. A., Kramer E. J., Marko J. F. and Bates F. S., *Macromolecules*, **26** (1993) 5566; Krausch G., Kramer E., Bates F. S., Marko J. F., Brown G. and Chakrabarti A., *Macromolecules*, **27** (1994) 6768.
[11] Ball R. C. and Essery R. L. H., *J. Phys. Condens. Matter*, **2** (1990) 10303.
[12] Brown G. and Chakrabarti A., *Phys. Rev. A*, **46** (1992) 4829; Brown G., Chakrabarti A. and Marko J. F., *Phys. Rev. E*, **50** (1994) 1674.
[13] Puri S. and Binder K., *Phys. Rev. A*, **46** (1992) R4487; *Phys. Rev. E*, **49** (1994) 5359.
[14] Marko J. F., *Phys. Rev. E*, **48** (1993) 2861.
[15] Siggia E. D., *Phys. Rev. A*, **20** (1979) 595.
[16] Wiltzius P. and Cumming A., *Phys. Rev. Lett.*, **66** (1991) 3000.
[17] Cumming A., Wiltzius P., Bates F. S. and Rosedale J. H., *Phys. Rev. A*, **45** (1992) 885; Shi B. Q., Harrison C. and Cumming A., *Phys. Rev. Lett.*, **70** (1993) 206; Harrison C., Rippard W. and Cumming A., *Phys. Rev. E*, **52** (1995) 723.
[18] Troian S. M., *Phys. Rev. Lett.*, **71** (1993) 1399; **72** (1994) 3739.
[19] Tanaka H., *Phys. Rev. Lett.*, **70** (1993) 2770.
[20] Tanaka H., *Phys. Rev. Lett.*, **72** (1994) 1702; *Phys. Rev. E*, **51** (1995) 1313.
[21] Tanaka H., *Phys. Rev. E*, **54** (1996) 1709.
[22] Liu A. J., Durian D. J., Herbolzheimer E. and Safran S. A., *Phys. Rev. Lett.*, **65** (1990) 1897.
[23] Guenoun P., Beysens D. and Robert M., *Phys. Rev. Lett.*, **65** (1990) 2406.
[24] Bodensohn J. and Goldburg W. I., *Phys. Rev. A*, **46** (1992) 5084.
[25] Tanaka H., *Phys. Rev. Lett.*, **70** (1993) 53.
[26] Tanaka H., *Europhys. Lett.*, **24** (1993) 665.
[27] Keblinski P., Ma W. J., Maritan A., Koplik J. and Banavar J., *Phys. Rev. E*, **47** (1993) R2265; *Phys. Rev. Lett.*, **72** (1994) 3738.
[28] Chen H. and Chakrabarti A., *Phys. Rev. E*, **55** (1997) 5680.
[29] San M. Miguel, Grant M. and Gunton J. D., *Phys. Rev. A*, **31** (1985) 1001.
[30] Pak H. K. and Law B. M., *Europhys. Lett.*, **31** (1995) 19.
[31] Tanaka H. and Araki T., *Phys. Rev. Lett.*, **81** (1998) 389.
[32] Wagner A. J. and Yeomans J. M., *Phys. Rev. Lett.*, **80** (1998) 1429.